Enhanced terrestrial weathering/runoff and surface ocean carbonate production during the recovery stages of the Paleocene-Eocene thermal maximum

D. Clay Kelly,[1] James C. Zachos,[2] Timothy J. Bralower,[3] and Stephen A. Schellenberg[4]

Received 6 April 2005; revised 15 July 2005; accepted 2 September 2005; published 17 December 2005.

[1] The carbonate saturation profile of the oceans shoaled markedly during a transient global warming event known as the Paleocene-Eocene thermal maximum (PETM) (circa 55 Ma). The rapid release of large quantities of carbon into the ocean-atmosphere system is believed to have triggered this intense episode of dissolution along with a negative carbon isotope excursion (CIE). The brevity (120–220 kyr) of the PETM reflects the rapid enhancement of negative feedback mechanisms within Earth's exogenic carbon cycle that served the dual function of buffering ocean pH and reducing atmospheric greenhouse gas levels. Detailed study of the PETM stratigraphy from Ocean Drilling Program Site 690 (Weddell Sea) reveals that the CIE recovery period, which postdates the CIE onset by ~80 kyr, is represented by an expanded (~2.5 m thick) interval containing a unique planktic foraminiferal assemblage strongly diluted by coccolithophore carbonate. Collectively, the micropaleontological and sedimentological changes preserved within the CIE recovery interval reflect a transient state when ocean-atmosphere chemistry fostered prolific coccolithophore blooms that suppressed the local lysocline to relatively deeper depths. A prominent peak in the abundance of the clay mineral kaolinite is associated with the CIE recovery interval, indicating that continental weathering/runoff intensified at this time as well (Robert and Kennett, 1994). Such parallel stratigraphic changes are generally consonant with the hypothesis that enhanced continental weathering/runoff and carbonate precipitation helped sequester carbon during the PETM recovery period (e.g., Dickens et al., 1997; Zachos et al., 2005).

Citation: Kelly, D. C., J. C. Zachos, T. J. Bralower, and S. A. Schellenberg (2005), Enhanced terrestrial weathering/runoff and surface ocean carbonate production during the recovery stages of the Paleocene-Eocene thermal maximum, *Paleoceanography*, *20*, PA4023, doi:10.1029/2005PA001163.

1. Introduction

[2] An ancient global warming event, referred to as the Paleocene-Eocene thermal maximum (PETM), punctuated Earth's climate history ~55 Ma. The onset of this climatic shift was particularly rapid (<several 10^3 years) given its extreme magnitude [*Kennett and Stott*, 1991; *Bralower et al.*, 1997; *Röhl et al.*, 2000; *Farley and Eltgroth*, 2003]: sea surface temperatures high and low latitudes increased above background levels by ~8°C and ~5°C respectively, oceanic intermediate water temperatures warmed by ~5°C, and temperate continental regions warmed by ~4°C [*Kennett and Stott*, 1991; *Bralower et al.*, 1995; *Fricke et al.*, 1998; *Zachos et al.*, 2001, 2003; *Tripati and Elderfield*, 2005]. Moreover, the environmental changes wrought by the PETM profoundly affected the global biosphere, altering biotic evolution among organisms ranging from marine protists to terrestrial vertebrates [*Koch et al.*, 1992, 1995; *Thomas and Shackleton*, 1996; *Kelly et al.*, 1996, 1998; *Schmitz et al.*, 1996; *Thomas*, 1998; *Clyde and Gingerich*, 1998; *Bowen et al.*, 2002; *Bralower*, 2002; *Gingerich*, 2003].

[3] Global carbon cycling was drastically perturbed during the PETM as reflected by an abrupt, negative carbon isotope excursion (CIE) recorded in both terrestrial materials and marine carbonates as well as by pervasive carbonate dissolution in the world oceans [*Kennett and Stott*, 1991; *Koch et al.*, 1992, 2003; *Thomas and Shackleton*, 1996; *Thomas et al.*, 1999; *Bowen et al.*, 2001; *Bralower et al.*, 2002; *Zachos et al.*, 2001, 2003, 2005; *Bains et al.*, 1999, 2003]. These lines of evidence indicate that vast amounts of isotopically light carbon (≫2000 Gt C) were injected into the ocean-atmosphere system. To date, the most parsimonious mechanism for the sudden release of large quantities of ^{12}C into Earth's surficial carbon reservoir is the catastrophic dissociation of sedimentary methane hydrate along continental slopes [*Dickens et al.*, 1995; *Katz et al.*, 1999], although increased mantle CO_2 outgassing and geothermal activity may have played an important role as well [*Rea et al.*, 1990; *Eldholm and Thomas*, 1993; *Svensen et al.*, 2004]. Regardless of source, a massive influx of

[1]Department of Geology and Geophysics, University of Wisconsin-Madison, Madison, Wisconsin, USA.
[2]Earth Sciences Department, University of California, Santa Cruz, California, USA.
[3]Department of Geosciences, Pennsylvania State University, University Park, Pennsylvania, USA.
[4]Department of Geological Sciences, San Diego State University, San Diego, California, USA.

0883-8305/05/2005PA001163$12.00

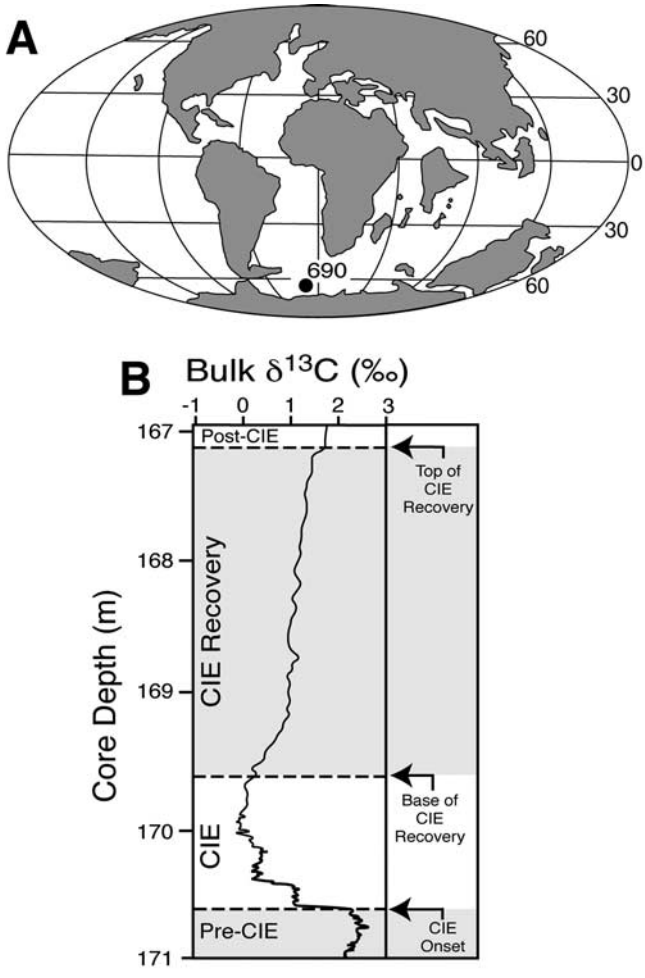

Figure 1. (a) Global map showing late Paleocene paleogeography and location of Site 690 in the Weddell Sea near Antarctica (from Ocean Drilling Stratigraphic Network). (b) Bulk carbonate $\delta^{13}C$ chemostratigraphy delineating the four stages of the CIE, most notably the expanded interval representing the CIE recovery period [data from *Bains et al.*, 1999]. See color version of this figure in the HTML.

carbon into the ocean-atmosphere system would have elevated pCO_2 levels thereby decreasing the carbonate ion concentration [CO_3^{2-}] of seawater, triggering a concomitant shoaling of the oceanic carbonate saturation horizon [*Dickens et al.*, 1997].

[4] The transient nature (~120–220 kyr) of PETM warmth, rapid removal of ^{12}C from the ocean-atmosphere system, and resumption of carbonate sedimentation following the CIE all indicate that negative feedback mechanisms within the global carbon cycle abated greenhouse climatic conditions [*Norris and Röhl*, 1997; *Röhl et al.*, 2000; *Farley and Eltgroth*, 2003; *Zachos et al.*, 2005]. A number of negative feedback processes may have contributed to carbon sequestration including expansion of continental vegetation with increased terrestrial organic carbon storage [*Beerling*, 2000] and/or elevated surface ocean productivity with increased marine organic carbon burial [*Bains et al.*, 2000]. However, quantitatively the most important feedback for permanently sequestering carbon and lowering atmospheric CO_2 levels is the acceleration of silicate-weathering reactions on land [e.g., *Walker et al.*, 1981; *Berner et al.*, 1983; *Sundquist*, 1991; *Kump and Arthur*, 1997]. This weathering mechanism would yield a net positive influx of bicarbonate and soluble cations into the ocean, thereby driving ocean carbonate content toward saturation and enhancing carbonate production/preservation until equilibrium was restored [*Dickens et al.*, 1995, 1997].

[5] Here we examine the micropaleontology and sedimentology of the CIE recovery interval preserved at Ocean Drilling Program (ODP) Site 690 to better delineate the relative timing and scale of local changes that unfolded amongst the calcareous plankton as the PETM waned. Site 690 has figured prominently in the study of the PETM [*Kennett and Stott*, 1991], and the bulk carbonate $\delta^{13}C$ record for this relatively expanded section is widely upheld as a benchmark for gauging the stratigraphic completeness of other deep-sea PETM sections [e.g., *Bains et al.*, 1999; *Röhl et al.*, 2000; *Farley and Eltgroth*, 2003]. Previous investigations of this record have focused primarily on the lower part of the CIE to document the initial responses of the marine biota and carbon cycle to the onset of PETM conditions [e.g., *Kennett and Stott*, 1991; *Bains et al.*, 2000; *Kelly*, 2002; *Bralower*, 2002; *Stoll and Bains*, 2003], while the uppermost portion of the CIE where $\delta^{13}C$ ratios gradually return to background values and carbonate content recovers has received scant attention [*Kelly*, 2002; *Farley and Eltgroth*, 2003]. Hence study of the CIE recovery interval from Site 690 should further elucidate (1) the dynamic interplay between the pelagic ecosystem and marine carbon cycling, (2) how these linked processes interacted to influence Site 690 PETM lithostratigraphy, and (3) the implications these records of change have for PETM negative feedback mechanisms.

2. Materials and Methods

[6] Site 690 is located atop Maud Rise in the South Atlantic sector (65°09′S, 01°12′E) of the Southern Ocean (Figure 1a). Late Paleocene benthic foraminiferal assemblages indicate a lower bathyal to upper abyssal paleobathymetry [*Thomas*, 1990]. Fifty-three samples were taken at moderate resolution (~10 cm) through 5.48 m of this PETM section (171.42–165.94 m), with the base of the sampling interval positioned well below the CIE onset, extending up section through the top of core 19 and into the bottom of overlying core 18. Prior to processing, a small portion (~4 cc) of each bulk sample was removed to accommodate study of calcareous nannofossil assemblages and weight percent $CaCO_3$ measurements. Weight percent $CaCO_3$ was determined from bulk powdered (<63 μm) aliquots (10–20 mg) via coulometric titration on an UIC Inc. Model 5240 automated-coulometrics device. Replicate analyses of a carbonate standard yielded an analytical precision of ±1%. Smear slide preparation and nannofossil counts were performed as described by *Bralower* [2002], samples were soaked in water until disaggregated, and nannofossil taxa

were identified using a light microscope at a magnification of 1250X. Previous study of nannofossil assemblages preserved within the lower half of the CIE demonstrated that these nannofloras are dominated (48–84%) by taxa belonging to the genus *Toweius*, which tended to mask relative abundance changes in other critical nannofossil genera [*Bralower*, 2002]. Consequently, an average of 250 "non-*Toweius*" specimens was counted on each slide to delineate relative abundance changes among such nannofossil genera as *Discoaster*, *Fasciculithus* and *Sphenolithus*.

[7] Samples for planktic foraminiferal assemblage and preservation studies were initially oven dried at 30°C and weighed prior to soaking in a weak (3%) peroxide solution. The disaggregated samples were gently rinsed with tap water over a 63-μm sieve, oven dried, and the weight of the coarse fraction (>63 μm) recorded. This technique minimized damage to shells and permitted calculation of weight percent coarse fraction for each sample, a useful proxy for gauging the relative proportion of foraminiferal shells preserved within deep-sea sediments [*Peterson and Prell*, 1985]. A split (>125 μm) of each sample was then examined to determine the relative proportions of shell fragments, broken shells and whole shells among planktic foraminiferal assemblages; such fragmentation data are routinely used to delineate stratigraphic changes in planktic foraminiferal preservation [e.g., *Thunell*, 1976; *Howard and Prell*, 1994; *Tedford and Kelly*, 2004]. Shell fragmentation is expressed as a percentage of the total sum of all grains (whole shells and fragments) counted in each sample. In general, a minimum of 250 whole shells was counted in each sample. Furthermore, the relative abundances of various planktic foraminiferal taxa were counted using a minimum of 250 specimens (>180 μm) in each sample. Taxa were classified into six broadly defined groups based upon phylogenetic relationships, paleoecological affinities, and/or stratigraphic distributions. For illustrative purposes, rare taxa (*Globanomalina australiformis*, *Chiloguembelina* spp.) with erratic stratigraphic distributions are assigned to a "miscellaneous" group.

[8] Stable isotope analyses ($\delta^{18}O$, $\delta^{13}C$) were performed on Micromass Prism and Optima mass spectrometers fitted with Autocarb devices at the University of California, Santa Cruz. Foraminiferal samples were reacted in a common phosphoric acid bath at 90°C. Replicate analyses of the laboratory standards NBS-19 and Carrara Marble (an in-house standard) established that average precision for samples smaller than 40 μg was 0.04‰ (1σ) for $\delta^{13}C$ and 0.06‰ (1σ) for $\delta^{18}O$ measurements. Suites of size-specific foraminifera were analyzed to construct a series of parallel stable isotope records. Shell size ranges and number of specimens used in each foraminiferal sample varied as follows: *Acarinina soldadoensis* (250–300 μm, 3–11 specimens), *A. subsphaerica* (150–250 μm, 15–20 specimens), *Subbotina* spp. (250–300 μm, 3–12 specimens), and *Nuttalides truempyi* (150–250 μm, 6–15 specimens). The absence of typical, mixed layer–dwelling acarininids within the CIE recovery interval necessitated the use of *A. subsphaerica*. This substitution is problematic since the preferred depth ecology of *A. subsphaerica* is highly variable [*Berggren and Norris*, 1997; *Olsson et al.*, 1999; *Quillévéré et al.*, 2001]. The stable isotope ratios of *Subbotina* spp. and the benthic taxon (*N. truempyi*) provide environmental information about thermocline and lower bathyal intermediate waters, respectively. The correction factors reported by *Katz et al.* [2003] were applied to measured *N. truempyi* $\delta^{18}O$ and $\delta^{13}C$ ratios to better approximate isotopic equilibrium with seawater. All supporting micropaleontological, stable isotope, and sedimentological data have been electronically archived with the World Data Center for Paleoclimatology.[1]

3. Results

[9] The high-resolution (centimeter scale), bulk carbonate $\delta^{13}C$ record generated by *Bains et al.* [1999] for the Site 690 section provides a useful chemostratigraphic framework for relating patterns of biotic and sedimentologic change to various stages of the PETM. To this end, we use the fine-scale structure of the CIE to delimit the following stratigraphic series of PETM stages: (1) "pre-CIE interval" (171.42–170.63 m) representing background conditions that existed prior to the CIE; (2) "CIE interval" (170.63–169.60 m) represents the core of the PETM from the CIE onset through to the level where isotopic ratios first begin to steadily increase; (3) "CIE recovery interval" (169.60–167.10 m) an expanded interval in which $\delta^{13}C$ ratios gradually return to higher, background values that typify the earliest Eocene; and (4) "post-CIE interval" (167.10–165.94 m) the uppermost portion of the study section that postdates the CIE and represents earliest Eocene conditions (Figure 1b).

3.1. Micropaleontology (Planktic Foraminifera and Calcareous Nannofossils)

[10] For comparative purposes, the micropaleontological data compiled from the CIE recovery interval have been spliced onto those previously published for the lower part of the CIE beginning at 169.55 m. The response of calcareous plankton to the onset of PETM conditions at Site 690 has already been documented [*Bralower*, 2002; *Kelly*, 2002], so we provide only a brief account for this part of the record. The base of the CIE interval is marked by the first occurrences of thermophilic planktic foraminifera (morozovellids and robust acarininids) and sharp increases in the relative abundances of warm water calcareous nannofossils (discoasters and fasciculiths) (Figure 2).

[11] A secondary response straddles (169.74–169.10 m) the transition between the CIE and CIE recovery intervals. This shift entailed pronounced increases in the abundances of robust, heavily calcified planktic foraminifera (*A. soldadoensis*, *A. coalingensis*) and the nannofossil genus *Sphenolithus*, while the relative abundances of the nannofossil genera *Discoaster* and *Fasciculithus* gradually declined (Figure 2). A major, transient turnover occurs among the planktic foraminifera within the CIE recovery interval. This

[1]Supporting data are electronically available at World Data Center for Paleoclimatology: NOAA Paleoclimatology Program, 325 Broadway, Code E/CC23, Boulder, CO 80305-3328, USA (paleo@noaa.gov; http://www.ncdc.noaa.gov/paleo/paleo.html).

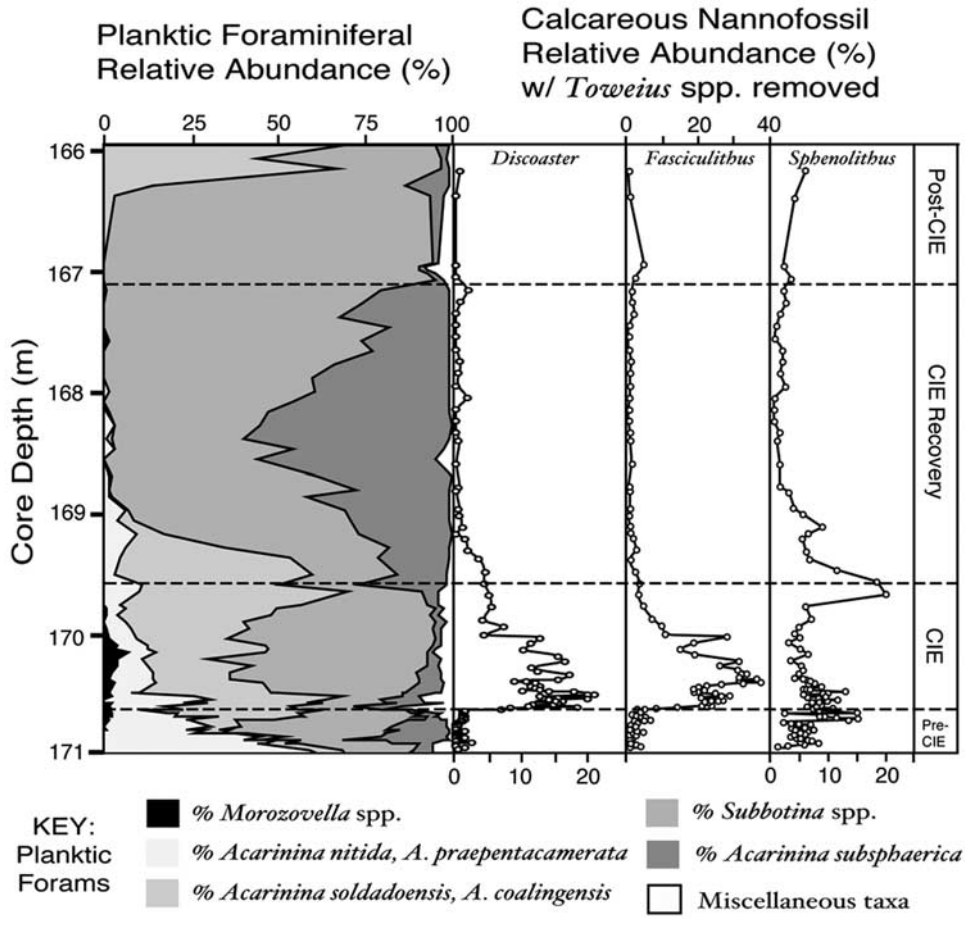

Figure 2. Stratigraphic variation in the relative abundances of different calcareous plankton groups within the Paleocene-Eocene thermal maximum (PETM) record from Site 690. (left) Stratigraphic patterns of change in the taxonomic compositions of planktic foraminiferal assemblages. Note *A. subsphaerica* acme is coincident with CIE recovery interval. (right) Stratigraphic variation in the relative abundances of calcareous nannofossil taxa as expressed by removing superabundant *Toweius* spp. Note steady decline of "nonplacolith" nannofossils (discoasters, fasciculiths, and sphenoliths) just prior to the CIE recovery interval.

short-lived faunal shift is delineated by 21 contiguous samples, and involved sharp decreases in the relative abundances of several acarininid species (*A. nitida*, *A. praepentacamerata*, *A. soldadoensis*, *A. coalingensis*) accompanied by a temporary increase in the relative abundance of high-spired *A. subsphaerica* (Figure 2). The *A. subsphaerica* acme is centered on 168.34 m where these variants compose nearly 60% of the assemblage.

[12] The *A. subsphaerica* acme is succeeded by a fourth faunal shift that is coincident with the termination of the CIE recovery interval (167.10 m) near the top of core 19. These post-CIE assemblages are composed almost entirely (~95%) of members of the genus *Subbotina*, and are found higher in the section within the bottom of core 18 (166.36 m). Nannofossil assemblages associated with both the *A. subsphaerica* and *Subbotina* acmes are characterized by a dearth of discoasters, fasciculiths and sphenoliths. Background planktic foraminiferal assemblages containing abundant (~67%) *A. soldadoensis* and *A. coalingensis* return immediately above the transient subbotinid acme at 166.14 m (Figure 2). The reestablishment of acarininid dominance is accompanied by a modest increase in the relative abundance of the nannofossil genus *Sphenolithus* (Figure 2).

3.2. Light Stable Isotopes

[13] Foraminiferal stable isotope data were generated to extend the existing, high-resolution records for the lower CIE [*Kennett and Stott*, 1991; *Thomas et al.*, 2002] up section through the entirety of the CIE recovery interval (169.60–166.90 m). Extension of the abbreviated *Acarinina* record through this critical interval of change was of primary importance (Figure 3a). The seven samples from the lowermost part of the CIE recovery interval (169.55–168.94 m) contain rare specimens of the surface-dwelling *A. soldadoensis*. Comparison of the stable isotope signa-

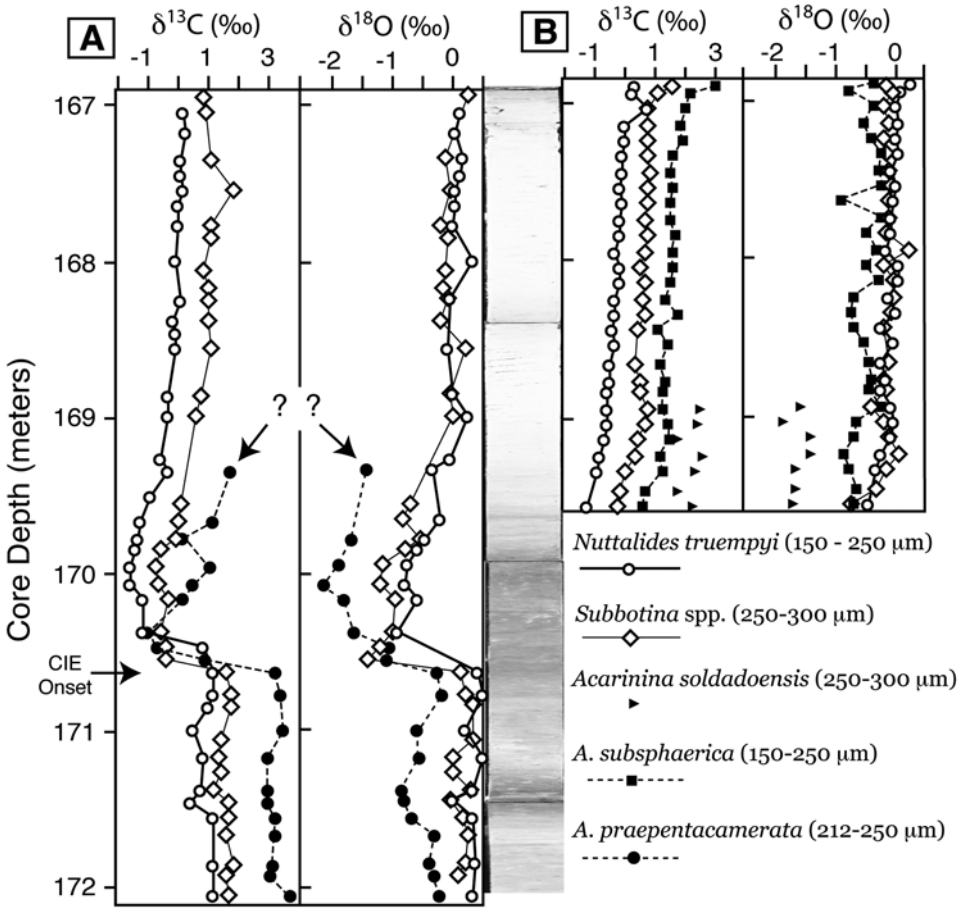

Figure 3. Parallel stable isotope records derived from various depth-stratified foraminiferal species through the PETM section of Site 690. (a) Original stable isotope record published by *Kennett and Stott* [1991]. Note sea surface (*A. praepentacamerata*) record does not extend up section into CIE recovery interval as indicated by question marks. (b) Complementary foraminiferal stable isotope record showing persistent interspecies $\delta^{13}C$ offsets and subtle increase in benthic foraminiferal $\delta^{18}O$ values through the CIE recovery interval. Reduced acarininid diversity within this interval necessitated use of *A. subsphaerica*. All stable isotope ratios are reported relative to Vienna Peedee belemnite (VPDB). See color version of this figure in the HTML.

tures of these *A. soldadoensis* to those of co-occurring *A. subsphaerica* revealed significant offsets (~1.0‰) between the two taxa, with the former species registering higher $\delta^{13}C$ and lower $\delta^{18}O$ ratios (Figure 3b).

[14] Furthermore, the $\delta^{13}C$ records of the three range-through foraminiferal taxa are consistently offset, with *A. subsphaerica* recording the highest ratios, *Subbotina* spp. being intermediate, and the benthic species (*N. truempyi*) registering the lowest ratios (Figure 3b). Ratios in all three of the foraminiferal $\delta^{13}C$ records steadily increase through the CIE recovery interval, with *A. subsphaerica* values increasing by ~2.0‰, *N. truempyi* values by ~1.6‰, and *Subbotina* spp values by ~1.0‰. The $\delta^{18}O$ ratios for the three range-through foraminiferal taxa converge multiple times (Figure 3b). The *Subbotina* spp. and benthic $\delta^{18}O$ records are indistinguishable, with both taxa recording gradual $\delta^{18}O$ increases of ~0.5‰ and ~0.7‰ respectively. The *A. subsphaerica* $\delta^{18}O$ values do not appear to change significantly.

3.3. Sedimentology and Planktic Foraminiferal Fragmentation

[15] Each of the CIE subdivisions possesses its own distinctive sedimentological signature, indicating that changes in the tempo and mode of sedimentation have influenced the structure of the CIE curve. Much of this sedimentological variation is also expressed by the color changes seen in the Site 690 stratigraphy (Figure 4a). The pre-CIE interval is typified by weight percent $CaCO_3$ values that fluctuate about a mean baseline of ~82%, weight percent coarse-fraction values varying between 5 and 9%, and a mean fragmentation value of ~11% (Figures 4b–4d). Weight percent $CaCO_3$ values begin to decline just below the base of the overlying CIE interval,

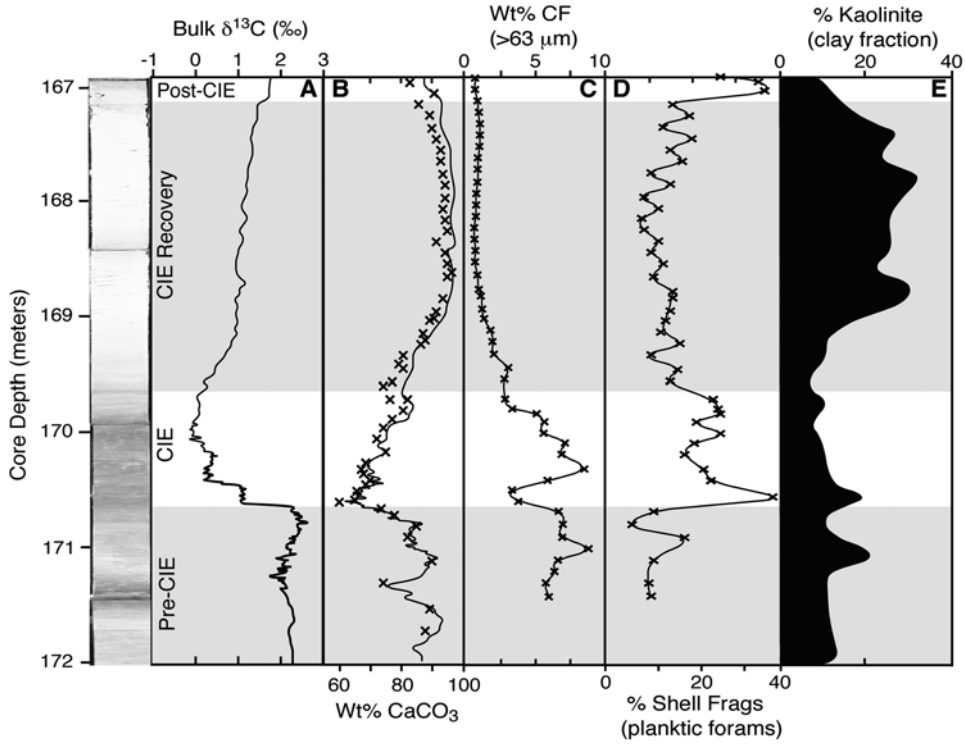

Figure 4. Patterns of stratigraphic variation in carbonate sedimentation and clay mineralogy within Site 690 PETM record. Note stark white color of CIE recovery interval shown in digital core photo at far left. (a) Bulk carbonate $\delta^{13}C$ chemostratigraphy delineating the various stages of the CIE, most notably the CIE recovery interval within the upper part of core [data from *Bains et al.*, 1999]. (b) Weight percent $CaCO_3$ data compared to high-resolution curve of *Farley and Eltgroth* [2003] showing enriched carbonate content of CIE recovery interval. (c) Weight percent coarse fraction record expressing scarcity of foraminiferal shells within carbonate-enriched, CIE recovery interval. (d) Stratigraphic changes in planktic foraminiferal shell fragmentation. (e) Stratigraphic variation in clay-mineral assemblages showing prominent peak in kaolinite abundance within the CIE recovery interval. Figure 4e is reprinted from *Robert and Kennett* [1994], with permission from Elsevier. See color version of this figure in the HTML.

registering a minimum value (59%) at the CIE onset (Figure 4b). The lower carbonate content and increased amount of clay imparts a reddish hue to the CIE interval. A transient decrease in weight percent coarse fraction and a sharp increase in planktic foraminiferal shell fragmentation (39%) accompany the CIE onset (Figures 4c and 4d).

[16] Carbonate preservation begins to improve within upper part of the CIE interval as reflected by higher weight percent $CaCO_3$ values and lower average fragmentation ($\sim$25%), although these fragmentation values are still relatively high. It is therefore surprising that weight percent coarse-fraction values start to decline during the CIE recovery as carbonate content and shell fragmentation continue to increase and decrease, respectively. The inverse relationship between weight percent coarse fraction and weight percent $CaCO_3$ is most strongly expressed within the upper part of the CIE recovery interval where the former declines into an extended minimum ($\leq$1 wt %) while the latter attains peak ($\geq$90 wt %) values (Figures 4b and 4c); average fragmentation values ($\sim$13%) are considerably lower within this interval as well (Figure 4d). The homogeneous, carbonate-rich, fine-grained character of the CIE recovery interval is expressed by its stark white color. In summary, the CIE recovery interval is typified by peak carbonate content, minimal amounts of coarse fraction (= few foraminiferal shells), improved foraminiferal preservation, and a unique planktic foraminiferal assemblage (= *A. subsphaerica* acme). This expanded portion of the Site 690 PETM stratigraphy is capped by a post-CIE interval that has slightly less carbonate ($\sim$85 wt %) and highly fragmented planktic foraminiferal assemblages ($\sim$33%) dominated by the genus *Subbotina* (Figures 4b and 4d).

4. Discussion

[17] The onset of the CIE at Site 690 is accompanied by a decline in both carbonate content and coarse fraction as well as increased levels of shell fragmentation (Figures 4a–4d). These lines of evidence indicate that the local lysocline shoaled with the initiation of the CIE, and support the interpretation that ocean acidification was initially neutralized by carbonate dissolution during the PETM [*Dickens et*

al., 1997]. However, the degree of PETM dissolution at Site 690 is not as severe as that seen in other records of comparable water depth. For instance, the lowest carbonate content (59 wt % $CaCO_3$) recorded in the Site 690 PETM section is much higher than that at Site 1263 in the southeastern Atlantic (paleobathymetry = 1500 m) where peak dissolution resulted in a layer of clay (<1 wt % $CaCO_3$) virtually devoid of carbonate [*Zachos et al.*, 2005]. The presence of considerably more carbonate within the interval of peak dissolution at Site 690 indicates that at no time during the PETM was this site below the calcite compensation depth (CCD). Such spatial variation in the degree of PETM dissolution likely reflects proximity to the carbon source (CO_2 or CH_4) in conjunction with where the liberated carbon was being transferred to the deep ocean via thermohaline circulation [e.g., *Feely et al.*, 2004]; a high carbonate flux may also depress the CCD locally.

[18] This pulse of intensified carbonate dissolution was followed by a gradual descent of the local lyscoline with carbonate preservation steadily improving as PETM conditions waned. It is within the ensuing CIE recovery interval (~169.60–166.90 m) that a remarkable series of parallel micropaleontological and sedimentological changes are recorded at Site 690. Among the planktic foraminifera, this episode of change is recorded as a transient yet pronounced turnover that entailed the temporary disappearance of several mixed layer–dwelling species belonging to the genus *Acarinina*. The conspicuous absences of *A. soldadoensis* and *A. coalingensis*, and high *A. subsphaerica* abundances makes this CIE recovery assemblage distinctly different from those found anywhere else in the study section (Figure 2). Thus the restricted stratigraphic range of the *A. subsphaerica* acme delimits a brief period when highly unusual sea surface conditions prevailed over Site 690.

[19] The stable isotopic signature of *A. subsphaerica* is unusual in that it is more similar to that of cool water subbotinids (Figure 3b). The relatively low $\delta^{13}C$ and high $\delta^{18}O$ ratios registered by *A. subsphaerica* indicate that this species either inhabited an unusually deep depth for an acarininid, or calicified its test during the winter months when sea surface temperatures were cooler. If one adopts the conventional view that the *A. subsphaerica* stable isotope signal reflects a deeper depth ecology [*Berggren and Norris*, 1997; *Quillévéré et al.*, 2001], then it follows that the oceanic mixed layer was temporarily devoid of planktic foraminifera during much of the CIE recovery period. This bizarre faunal response may be viewed as a form of ecological opportunism whereby *A. subsphaerica* flourished and/or some type of ecological exclusion that temporarily eliminated local populations of *A. soldadoensis* and *A. coalingensis*.

[20] The *A. subsphaerica* acme is eventually succeeded by post-CIE planktic foraminiferal assemblages dominated (>90%) by cool water subbotinids. This conspicuous phase of subbotinid dominance coincides with a sharp increase in shell fragmentation (~33%), and is correlative with the end of the CIE recovery interval (167.10 m) near the top of core 19 (Figures 2 and 4d). Background planktic foraminiferal assemblages containing typical, mixed layer dwellers (*A. soldadoensis* and *A. coalingensis*) do not return until further up section within the bottom of core 18 (166.26 m), suggesting that the environmental "fallout" and biotic effects of the PETM lingered beyond the CIE recovery period.

4.1. Implications for PETM Age Models and Paleoproductivity Records

[21] Two age models have been constructed for the Site 690 PETM record: a cyclostratigraphic model based on precessional-scale (21 kyr) variation in sedimentary Fe and Ca contents [*Röhl et al.*, 2000], and an alternative chronology predicated upon a constant flux of cosmogenic ^3He to the seafloor [*Farley and Eltgroth*, 2003]. These two chronologies are generally congruent, with both reflecting a rapid (<several kyr) CIE onset followed by ~80 kyr of peak PETM conditions. However, significant differences emerge between the two age models with respect to the duration of the ensuing CIE recovery interval. The orbital age model estimates that this interval represents ~140 kyr, while the ^3He age model yields an estimate of only ~30 kyr. Both age models call for increased sedimentation rates through the CIE recovery interval, but the increase predicted by the ^3He age model is especially pronounced (~10 cm/kyr). Several lines of evidence indicate that sedimentation rates increased within the CIE recovery interval, most notably extreme carbonate dilution dampens both the sedimentary Fe cycles, a serious setback for the orbital age model, and cosmogenic ^3He concentrations [*Röhl et al.*, 2000; *Farley and Eltgroth*, 2003].

[22] Here we note that this temporal discrepancy corresponds to the *A. subsphaerica* acme preserved within the CIE recovery interval. This stratigraphic interval has a carbonate content (>90%) that exceeds pre-CIE levels, yet its trivial (≤1) wt % coarse fraction reflects a surprisingly low foraminiferal shell content (Figures 4a–4c). This fine-grained deposit is not a product of size-selective sediment focusing by bottom water currents because such a taphonomic process cannot account for the unique faunal composition of the *A. subsphaerica* acme. In addition, planktic foraminiferal shells within this fine-grained deposit exhibit only minor degrees of fragmentation (~13%), precluding the possibility that this sedimentological shift is an artifact of selective dissolution (Figure 4d). The scarcity of foraminiferal shells within the carbonate-rich, CIE recovery interval is therefore attributed to a dilution effect caused by enhanced production/preservation of fine-fraction, coccolithophorid carbonate [*Kelly*, 2002]. Increased coccolithophorid carbonate production would also explain why the relative abundances of such "nonplacolith" nannofossil genera as discoasters, fasciculiths and sphenoliths decline within the CIE recovery interval (Figure 2).

[23] Numerical models designed to simulate the response of modern, marine carbonate chemistry to CIE-sized methane and anthropogenic CO_2 injections predict that several 100 kyr is required for all of the released carbon to be neutralized [*Walker and Kasting*, 1992; *Dickens et al.*, 1997; *Archer et al.*, 1997]. However, ocean carbonate chemistry can recover more rapidly in models that couple silicate weathering rates to climate [*Dickens et al.*, 1997]

than in models with fixed weathering rates [*Archer et al.*, 1997]. Thus the ^{3}He-based age model tends to favor models with negative feedbacks that vary with climate, while the orbital age model would favor those with fixed-rate feedbacks. Though we are unable to determine which of the two age models is most accurate, we note that the temporal discrepancy regarding the CIE recovery interval coincides with the *A. subsphaerica* acme and provide sedimentological evidence for enhanced coccolithophore calcification/preservation as the source of this fine-grained, carbonate influx.

[24] Increased surface ocean productivity with a strengthened biological pump has been proposed as a means of lowering atmospheric CO_2 levels during the PETM [*Bains et al.*, 2000; *Stoll and Bains*, 2003]. However, these paleoproductivity records appear to be out of phase with the pattern of carbonate sedimentation preserved at Site 690. Mass accumulation rates for biogenic barite decrease to background levels within the CIE recovery interval, suggesting that this episode of enhanced carbonate sedimentation unfolded as surface ocean productivity declined [*Bains et al.*, 2000]. These two lines of evidence are at odds, and we posit that this temporal discrepancy likely stems from the dilution of particulate organic carbon, the very medium upon which barite crystals precipitate, by a marked increase in the flux of inorganic carbon from the overlying surface ocean. Hence our findings underscore how changes to the sources and fluxes of surface ocean carbonate production influence lithostratigraphic geochemical variations, and highlight the importance of such data for evaluating astronomically tuned age models and paleoproductivity records [e.g., *Norris and Röhl*, 1997; *Röhl et al.*, 2000; *Bains et al.*, 2000].

4.2. Coupling of Continental Weathering/Runoff and Carbonate Sedimentation?

[25] The temporary disappearance of typical, mixed layer acarininids has adversely affected published stable isotope records for the Site 690 PETM section. Specifically, the sea surface record (= *Acarinina praepentacamerata*) of *Kennett and Stott* [1991] does not extend up through the CIE recovery interval; instead, it terminates at a stratigraphic level (169.33 m) roughly correlative with the base of the *A. subsphaerica* acme and the onset of improved carbonate preservation (Figure 3a). Our foraminiferal stable isotope data bridge this gap, and show that water column $\delta^{13}C$ gradients persisted as lower bathyal/upper abyssal waters cooled by $\sim$3°C during the CIE recovery. The persistent nature of such interspecies $\delta^{13}C$ offsets seems inconsistent with vigorous upwelling as a causal mechanism for the micropaleontological and sedimentological changes associated with the *A. subsphaerica* acme because intense upwelling tends to diminish such $\delta^{13}C$ gradients by pumping ^{12}C-enriched, intermediate water up into the overlying mixed layer. Thus we seek an alternative explanation for the genesis of the *A. subsphaerica* acme.

[26] One possibility is that enhanced chemical weathering/pedogenesis of the continents and increased riverine runoff fostered the *A. subsphaerica* acme and its associated coccolithophore blooms [e.g., *Bains et al.*, 2000; *Zachos and Dickens*, 2000]. This mechanism has been invoked to account for anomalous dinoflagellate blooms preserved in marginal marine settings during the PETM [*Crouch et al.*, 2001], and is consistent with PETM climate models and proxies that hindcast elevated levels of precipitation over the continents [*Huber and Sloan*, 1999; *Bowen et al.*, 2004]. Moreover, a coupled system binding chemical weathering of silicate rocks on land to deep-sea carbonate sedimentation has long been envisaged as a means of moderating atmospheric greenhouse gas levels and neutralizing ocean acidification [e.g., *Walker et al.*, 1981; *Berner et al.*, 1983; *Sundquist*, 1991; *Kump and Arthur*, 1997].

[27] Several lines of evidence indicate that chemical weathering rates increased during the PETM. The osmium isotopic ($^{187}Os/^{188}Os$) composition of seawater becomes more radiogenic during the PETM, a pattern of isotopic variation consistent with an accelerated hydrologic cycle and increased continental weathering/runoff [*Ravizza et al.*, 2001]. Furthermore, a warmer/wetter PETM climate state would have been conducive to the production of thermodynamically stable clays. Indeed, a prominent peak in the abundance of kaolinite coincides with the *A. subsphaerica* acme at Site 690 (Figure 4e). This clay-mineralogical shift is believed to signify increased Antarctic weathering/runoff [*Robert and Kennett*, 1992, 1994]. Similar spikes in kaolinite abundance have been noted in other geographically widespread PETM sections [e.g., *Gibson et al.*, 1993, 2000; *Kaiho et al.*, 1996; *Cramer et al.*, 1999; *Bolle and Adatte*, 2001], but the detrital nature of the kaolinite has left open the possibility that this clay-mineralogical shift simply reflects increased erosion/redeposition of preexisting kaolinite [e.g., *Thiry*, 2000]. Nevertheless, the coincidence of peak kaolinite abundances, increased coccolithophore carbonate sedimentation, and the *A. subsphaerica* acme all within the CIE recovery interval constitute compelling evidence for a direct relationship between intensified chemical weathering/runoff on the continents and enhanced carbonate sedimentation in the ocean.

[28] In theory, accelerated silicate weathering will yield a net positive flux of bicarbonate and soluble calcium and magnesium cations to the oceans thereby increasing carbonate saturation, which promotes precipitation of biogenic calcite [e.g., *Walker et al.*, 1981; *Berner et al.*, 1983; *Sundquist*, 1991]. Such a boost to carbonate production should suppress the lysocline/CCD to deeper depths and manifest itself as a stratigraphic interval of enhanced carbonate preservation within deep-sea sedimentary sequences [e.g., *Broecker et al.*, 1993]. Moreover, a spike in carbonate preservation is consistent with models that predict a transient deepening of the lysocline to depths deeper than initial levels as the ocean-atmosphere system recovers from an abrupt, large-scale carbon injection event [*Walker and Kasting*, 1992; *Dickens et al.*, 1997]. This predicted pattern of carbonate preservation was recently confirmed by drilling of a depth transect along the Walvis Ridge in the southeastern Atlantic [*Zachos et al.*, 2005]. The pattern of carbonate sedimentation preserved within the Site 690 PETM record is grossly compatible with such a lysocline "overdeepening"; carbonate content within the CIE recovery interval is higher than in the pre-CIE interval (Figure 4b). This interpretation,

however, is deemed provisional because a depth transect of PETM sites spanning the full range of lysocline movement is lacking for this region. We also note that while the decline in fragmentation within the CIE recovery interval is consistent with a deepening of the lysocline/CCD, the values are not much different than those from the pre-CIE interval.

5. Conclusions

[29] The PETM record recovered from Site 690 has been the focus of considerable scrutiny over the years; nevertheless, detailed study of its CIE recovery interval yields new insight into possible negative feedback mechanisms that acted to stabilize the ocean-climate system in the aftermath of this extraordinary global perturbation. Planktic foraminiferal assemblages from within the CIE recovery interval are unique in that they are dominated by *Acarinina subsphaerica* and lack typical, mixed layer species. The limited stratigraphic range of this short-lived *A. subsphaerica* acme indicates that atypical sea surface conditions temporarily prevailed throughout the Weddell Sea during the CIE recovery period. Furthermore, the *A. subsphaerica* acme is restricted to a stratigraphic interval characterized by enhanced carbonate sedimentation, diluted foraminiferal shell content, and high kaolinite abundances. The coincidence of these changes is taken to reflect a transient state when increased continental weathering/runoff fueled prolific coccolithophorid blooms that in turn suppressed the local lysocline to relatively deeper depths. Though this CIE recovery interval is characterized by peak carbonate content and decreased planktic foraminiferal fragmentation, we are unable to determine whether the lysocline descended to depths significantly deeper than pre-CIE levels because our study is limited to only a single, relatively shallow site. We also note that the increased flux of surface ocean carbonate strongly influenced lithostratigraphic geochemical variation, which underscores the importance of such sedimentological data to understanding PETM age models and paleoproductivity records [e.g., *Norris and Röhl*, 1997; *Röhl et al.*, 2000; *Bains et al.*, 2000; *Farley and Eltgroth*, 2003]. In summary, the parallel micropaleontological and sedimentological changes associated with the CIE recovery interval at Site 690 are generally consonant with the hypothesis that increased continental weathering/pedogenesis and riverine runoff helped neutralize ocean acidification during the later stages of the PETM.

[30] **Acknowledgments.** This research was funded by National Science Foundation (NSF) grants to D.C.K. and S.A.S. (OCE-0452253) and J.C.Z. and T.J.B. (EAR-0120727). Samples provided by the Ocean Drilling Program (ODP) were used in this study; ODP is funded through the NSF under management of Joint Oceanographic Institutions (JOI), Inc. The insightful reviews of David Hodell and David Archer improved this manuscript. We thank Gar Esmay and the curatorial staff at ODP-ECR for their assistance.

References

Archer, D., H. Kheshgi, and E. Maier-Reimer (1997), Multiple timescales for neutralization of fossil fuel CO_2, *Geophys. Res. Lett.*, *24*, 405–408.

Bains, S., R. M. Corfield, and R. D. Norris (1999), Mechanisms of climate warming at the end of the Paleocene, *Science*, *285*, 724–727.

Bains, S., R. D. Norris, R. M. Corfield, and K. L. Faul (2000), Termination of global warmth at the Palaeocene/Eocene boundary through productivity feedback, *Nature*, *407*, 171–174.

Bains, S., R. D. Norris, R. M. Corfield, G. J. Bowen, P. D. Gingerich, and P. L. Koch (2003), Marine-terrestrial linkages at the Paleocene-Eocene boundary, in *Causes and Consequences of Globally Warm Climates in the Early Paleogene*, edited by S. L. Wing, P. D. Gingerich, and B. Schmitz, *Spec. Pap. Geol. Soc. Am.*, *369*, 1–9.

Beerling, D. J. (2000), Increased terrestrial carbon storage across the Palaeocene-Eocene boundary, *Palaeogeogr. Palaeoclimatol. Palaeoecol.*, *161*, 395–405.

Berggren, W. A., and R. D. Norris (1997), Biostratigraphy, phylogeny and systematics of Paleocene trochospiral planktic foraminifera, *Micropaleontology*, *43*, suppl. 1, 116 pp.

Berner, R. A., A. C. Lasaga, and R. M. Garrels (1983), The carbonate-silicate geochemical cycle and its effect on atmospheric carbon dioxide over the past 100 million years, *Am. J. Sci.*, *283*, 641–683.

Bolle, M.-P., and T. Adatte (2001), Palaeocene-early Eocene climatic evolution in the Tethyan realm: Clay mineral evidence, *Clay Miner.*, *36*, 249–261.

Bowen, G. J., P. L. Koch, P. D. Gingerich, R. D. Norris, S. Bains, and R. M. Corfield (2001), Refined isotope stratigraphy across the continental Paleocene-Eocene boundary on Polecat Bench in the northern Bighorn Basin, in *Paleocene-Eocene Stratigraphy and Biotic Change in the Bighorn and Clarks Fork Basins, Wyoming*, edited by P. D. Gingerich, *Pap. Paleontol.*, vol. 33, pp. 73–88, Univ. of Mich., Ann Arbor.

Bowen, G. J., W. C. Clyde, P. L. Koch, S. Ting, J. Alroy, T. Tsubamoto, and Y. Wang (2002), Mammalian dispersal at the Paleocene/Eocene boundary, *Science*, *295*, 2062–2065.

Bowen, G. J., D. J. Beerling, P. L. Koch, J. C. Zachos, and T. Quattlebaum (2004), A humid climate state during the Palaeocene/Eocene thermal maximum, *Nature*, *432*, 495–499.

Bralower, T. J. (2002), Evidence of surface water oligotrophy during the Paleocene-Eocene thermal maximum: Nannofossil assemblage data from Ocean Drilling Program Site 690, Maud Rise, Weddell Sea, *Paleoceanography*, *17*(2), 1023, doi:10.1029/2001PA000662.

Bralower, T. J., J. C. Zachos, E. Thomas, M. Parrow, C. K. Paull, D. C. Kelly, I. Premoli Silva, W. V. Sliter, and K. C. Lohmann (1995), Late Paleocene to Eocene paleoceanography of the equatorial Pacific Ocean: Stable isotopes recorded at ODP Site 865, Allison Guyot, *Paleoceanography*, *10*, 841–865.

Bralower, T. J., D. J. Thomas, J. C. Zachos, M. M. Hirschmann, U. Röhl, H. Sigurdsson, E. Thomas, and D. L. Whitney (1997), High-resolution records of the late Paleocene thermal maximum and circum-Caribbean volcanism: Is there a causal link?, *Geology*, *25*, 963–967.

Bralower, T. J., I. Premoli-Silva, M. J. Malone, and the Scientific Party of Leg 198 (2002), New evidence for abrupt climate change in the Cretaceous and Paleogene: An Ocean Drilling Program expedition to Shatsky Rise, northwest Pacific, *GSA Today*, *12*, 4–10.

Broecker, W. S., Y. Lao, M. Klas, E. Clark, G. Bonani, S. Ivy, and C. Chen (1993), A search for an early Holocene $CaCO_3$ preservation event, *Paleoceanography*, *8*, 333–339.

Clyde, W. C., and P. D. Gingerich (1998), Mammalian community response to the latest Paleocene thermal maximum: An isotaphonomic study in the northern Bighorn Basin, Wyoming, *Geology*, *26*, 1011–1014.

Cramer, B. S., M.-P. Aubry, K. G. Miller, R. K. Olsson, J. D. Wright, and D. V. Kent (1999), An exceptional chronologic, isotopic, and clay mineralogic record of the latest Paleocene thermal maximum, Bass River, N. J., ODP 174AX, *Bull. Soc. Geol. Fr.*, *170*, 883–897.

Crouch, E. M., C. Heilmann-Clausen, H. Brinkhuis, H. E. G. Morgans, K. M. Rogers, H. Egger, and B. Schmitz (2001), Global dinoflagellate event associated with the late Paleocene thermal maximum, *Geology*, *29*, 315–318.

Dickens, G. R., J. R. O'Neil, D. K. Rea, and R. M. Owen (1995), Dissociation of oceanic methane hydrate as a cause of the carbon isotope excursion at the end of the Paleocene, *Paleoceanography*, *10*, 965–971.

Dickens, G. R., M. M. Castillo, and J. C. G. Walker (1997), A blast of gas in the latest Paleocene: Simulating first-order effects of

massive dissociation of oceanic methane hydrate, *Geology*, *25*, 259–262.
Eldholm, O., and E. Thomas (1993), Environmental impact of volcanic margin formation, *Earth Planet. Sci. Lett.*, *117*, 319–329.
Farley, K. A., and S. F. Eltgroth (2003), An alternative age model for the Paleocene-Eocene thermal maximum using extraterrestrial ^{3}He, *Earth Planet. Sci. Lett.*, *208*, 135–148.
Feely, R. A., C. L. Sabine, K. Lee, W. Berelson, J. Kleypas, V. J. Fabry, and F. J. Millero (2004), Impact of anthropogenic CO_2 on the $CaCO_3$ system in the oceans, *Science*, *305*, 362–366.
Fricke, H. C., W. C. Clyde, J. R. O'Neil, and P. D. Gingerich (1998), Evidence for rapid climate change in North America during the late Paleocene thermal maximum: Oxygen isotope compositions of biogenic phosphate from the Bighorn Basin (Wyoming), *Earth Planet. Sci. Lett.*, *160*, 193–208.
Gibson, T. G., L. M. Bybell, and J. P. Owens (1993), Latest Paleocene lithologic and biotic events in neritic deposits of southwestern New Jersey, *Paleoceanography*, *8*, 495–514.
Gibson, T. G., L. M. Bybell, and D. B. Mason (2000), Stratigraphic and climatic implications of clay mineral changes around the Paleocene/Eocene boundary of the northeastern U.S. margin, *Sediment. Geol.*, *134*, 65–92.
Gingerich, P. D. (2003), Mammalian responses to climate change at the Paleocene-Eocene boundary: Polecat Bench record in the northern Bighorn Basin, Wyoming, in *Causes and Consequences of Globally Warm Climates in the Early Paleogene*, edited by S. L. Wing, P. D. Gingerich, and B. Schmitz, *Geol. Soc. Am. Spec. Pap.*, *369*, 463–478.
Howard, W. R., and W. L. Prell (1994), Late Quaternary $CaCO_3$ production and preservation in the Southern Ocean: Implications for oceanic and atmospheric carbon cycling, *Paleoceanography*, *9*, 453–482.
Huber, M., and L. C. Sloan (1999), Warm climate transitions: A general circulation modeling study of the late Paleocene thermal maximum (~56 Ma), *J. Geophys. Res.*, *104*, 16,633–16,655.
Kaiho, K., et al. (1996), Latest Paleocene benthic foraminiferal extinction and environmental changes at Tawanui, New Zealand, *Paleoceanography*, *11*, 447–465.
Katz, M. E., D. K. Pak, G. R. Dickens, and K. G. Miller (1999), The source and fate of massive carbon input during the latest Paleocene thermal maximum, *Science*, *286*, 1531–1533.
Katz, M. E., D. R. Katz, J. D. Wright, K. G. Miller, D. K. Pak, N. J. Shackleton, and E. Thomas (2003), Early Cenozoic benthic foraminiferal isotopes: Species reliability and interspecies correction factors, *Paleoceanography*, *18*(2), 1024, doi:10.1029/2002PA000798.
Kelly, D. C. (2002), Response of Antarctic (ODP Site 690) planktonic foraminifera to the Paleocene-Eocene thermal maximum: Faunal evidence for ocean/climate change, *Paleoceanography*, *17*(4), 1071, doi:10.1029/2002PA000761.
Kelly, D. C., T. J. Bralower, J. C. Zachos, I. Premoli Silva, and E. Thomas (1996), Rapid diversification of planktonic foraminifera in the tropical Pacific (ODP Site 865) during the late Paleocene thermal maximum, *Geology*, *24*, 423–426.
Kelly, D. C., T. J. Bralower, and J. C. Zachos (1998), Evolutionary consequences of the latest Paleocene thermal maximum for tropical planktonic foraminifera, *Palaeogeogr. Palaeoclimatol. Palaeoecol.*, *141*, 139–161.
Kennett, J. P., and L. D. Stott (1991), Abrupt deep-sea warming, palaeoceanographic changes and benthic extinctions at the end of the Palaeocene, *Nature*, *353*, 225–229.
Koch, P. L., J. C. Zachos, and P. D. Gingerich (1992), Coupled isotopic change in marine and continental carbon reservoirs at the Palaeocene/Eocene boundary, *Nature*, *358*, 319–322.
Koch, P. L., J. C. Zachos, and D. L. Dettman (1995), Stable isotope stratigraphy and paleoclimatology of the Paleogene Bighorn Basin, *Palaeogeogr. Palaeoclimatol. Palaeoecol.*, *115*, 61–89.
Koch, P. L., W. C. Clyde, R. P. Hepple, M. L. Fogel, S. L. Wing, and J. C. Zachos (2003), Carbon and oxygen isotope records from paleosols spanning the Paleocene-Eocene boundary, Bighorn Basin, Wyoming, in *Causes and Consequences of Globally Warm Climates in the Early Paleogene*, edited by S. L. Wing, P. D. Gingerich, and B. Schmitz, *Spec. Pap. Geol. Soc. Am.*, *369*, 49–64.
Kump, L. R., and M. A. Arthur (1997), Global chemical erosion during the Cenozoic: Weatherability balances the budget, in *Tectonic Uplift and Climate Change*, edited by W. Ruddiman, pp. 399–426, Springer, New York.
Norris, R. D., and U. Röhl (1999), Carbon cycling and chronology of climate warming during the Palaeocene/Eocene transition, *Nature*, *401*, 775–778.
Olsson, R. K., C. Hemleben, W. A. Berggren, and B. T. Huber (1999), *Atlas of Paleocene Planktonic Foraminifera*, *Smithsonian Contrib. Paleobiol.*, vol. 85, 252 pp., Smithsonian Inst., Washington, D. C.
Peterson, L. C., and W. L. Prell (1985), Carbonate preservation and rates of climate change: An 800 kyr record from the Indian Ocean, in *The Carbon Cycle and Atmospheric CO_2: Natural Variation Archean to Present*, *Geophys. Monogr. Ser.*, vol. 32, edited by E. T. Sundquist and W. S. Broecker, pp. 251–269, AGU, Washington, D. C.
Quillévéré, F., R. D. Norris, I. Moussa, and W. A. Berggren (2001), Role of photosymbiosis and biogeography in the diversification of early Paleogene acarininids (planktonic foraminifera), *Paleobiology*, *27*, 311–326.
Ravizza, G., R. D. Norris, and J. Blusztajn (2001), An osmium isotope excursion associated with the late Paleocene thermal maximum: Evidence of intensified chemical weathering, *Paleoceanography*, *16*, 155–163.
Rea, D. K., J. C. Zachos, R. M. Owen, and P. D. Gingerich (1990), Global change at the Paleocene-Eocene boundary: Climatic and evolutionary consequences of tectonic events, *Palaeogeogr. Palaeoclimatol. Palaeoecol.*, *79*, 117–128.
Robert, C., and J. P. Kennett (1992), Paleocene and Eocene kaolinite distribution in the South Atlantic and Southern Ocean: Antarctic climatic and paleoceanographic implications, *Mar. Geol.*, *103*, 99–110.
Robert, C., and J. P. Kennett (1994), Antarctic subtropical humid episode at the Paleocene-Eocene boundary: Clay mineral evidence, *Geology*, *22*, 211–214.
Röhl, U., T. J. Bralower, R. D. Norris, and G. Wefer (2000), New chronology for the late Paleocene thermal maximum and its environmental implications, *Geology*, *28*, 927–930.
Schmitz, B., R. P. Speijer, and M.-P. Aubry (1996), Latest Paleocene benthic extinction event on the southern Tethyan shelf (Egypt): Foraminiferal stable isotopic ($\delta^{13}C$, $\delta^{18}O$) records, *Geology*, *24*, 347–350.
Stoll, H. M., and S. Bains (2003), Coccolith Sr/Ca records of productivity during the Paleocene-Eocene thermal maximum from the Weddell Sea, *Paleoceanography*, *18*(2), 1049, doi:10.1029/2002PA000875.
Sundquist, E. T. (1991), Steady- and non-steady-state carbonate-silicate controls on atmospheric CO_2, *Quat. Sci. Rev.*, *10*, 283–296.
Svensen, H., S. Planke, A. Malthe-Sørenssen, B. Jamtveit, R. Myklebust, T. R. Eidem, and S. S. Rey (2004), Release of methane from a volcanic basin as a mechanism for initial Eocene global warming, *Nature*, *429*, 542–545.
Tedford, R. A., and D. C. Kelly (2004), A deep-sea record of the late Miocene carbon shift from the southern Tasman Sea, in *The Cenozoic Southern Ocean: Tectonics, Sedimentation, and Climate Change Between Australia and Antarctica*, *Geophys. Monogr. Ser.*, vol. 151, edited by N. Exon, J. P. Kennett, and M. Malone, pp. 273–290, AGU, Washington, D. C.
Thiry, M. (2000), Palaeoclimatic interpretation of clay minerals in marine deposits: An outlook from the continental origin, *Earth Sci. Rev.*, *49*, 201–221.
Thomas, D. J., T. J. Bralower, and J. C. Zachos (1999), New evidence for subtropical warming during the late Paleocene thermal maximum: Stable isotopes from Deep Sea Drilling Project Site 527, Walvis Ridge, *Paleoceanography*, *14*, 561–570.
Thomas, D. J., J. C. Zachos, T. J. Bralower, E. Thomas, and S. Bohaty (2002), Warming the fuel for the fire: Evidence for the thermal dissociation of methane hydrate during the Paleocene-Eocene thermal maximum, *Geology*, *30*, 1067–1070.
Thomas, E. (1990), Late Cretaceous through Neogene deep-sea benthic foraminifers (Maud Rise, Weddell Sea, Antarctica), *Proc. Ocean Drill. Program Sci. Results*, *113*, 571–594.
Thomas, E. (1998), Biogeography of the late Paleocene benthic foraminiferal extinction, in *Late Paleocene-Early Eocene Climatic and Biotic Events in the Marine and Terrestrial Records*, edited by M.-P. Aubry, S. G. Lucas, and W. A. Berggren, pp. 214–235, Columbia Univ. Press, New York.
Thomas, E., and N. J. Shackleton (1996), The Paleocene-Eocene benthic foraminiferal extinction and stable isotope anomalies, in *Correlation of the Early Paleogene in Northwest Europe*, edited by R. W. O'B. Knox, R. M. Corfield, and R. E. Dunay, *Geol. Soc. Spec. Publ.*, *101*, 401–441.
Thunell, R. C. (1976), Optimal indices of calcium carbonate dissolution in deep-sea sediments, *Geology*, *4*, 525–528.
Tripati, A., and H. Elderfield (2005), Deep-sea temperature and circulation changes at the Paleocene-Eocene thermal maximum, *Science*, *308*, 1894–1898.
Walker, J. C. G., and J. F. Kasting (1992), Effects of fuel and forest conservation on future levels of atmospheric carbon dioxide, *Palaeogeogr. Palaeoclimatol. Palaeoecol.*, *97*, 151–189.
Walker, J. C. G., P. B. Hays, and J. F. Kasting (1981), A negative feedback mechanism for the long-term stabilization of Earth's surface temperature, *J. Geophys. Res.*, *86*(C10), 9776–9782.
Zachos, J. C., and G. R. Dickens (2000), An assessment of the biogeochemical feedback response to the climatic and chemical perturbations of the LPTM, in *Early Paleogene Warm*

Climates and Biosphere Dynamics, edited by B. Schmitz, B. Sundquist, and F. Andreasson, *GFF*, *122*(1), 188–189.

Zachos, J. C., M. Pagani, L. Sloan, E. Thomas, and K. Billups (2001), Trends, rhythms, and aberrations in global climate 65 Ma to present, *Science*, *292*, 686–693.

Zachos, J. C., M. W. Wara, S. Bohaty, M. L. Delaney, M. R. Petrizzo, A. Brill, T. J. Bralower, and I. Premoli-Silva (2003), A transient rise in tropical sea surface temperature during the Paleocene-Eocene thermal maximum, *Science*, *302*, 1551–1554.

Zachos, J. C., et al. (2005), Rapid acidification of the ocean during the Paleocene-Eocene thermal maximum, *Science*, *308*, 1611–1615.

T. J. Bralower, Department of Geosciences, Pennsylvania State University, University Park, PA 16802, USA.

D. C. Kelly, Department of Geology and Geophysics, University of Wisconsin, 1215 W. Dayton Street, Madison, WI 53706, USA. (ckelly@geology.wisc.edu)

S. A. Schellenberg, Department of Geological Sciences, San Diego State University, 5500 Campanile Drive, San Diego, CA 92182, USA.

J. C. Zachos, Earth Sciences Department, University of California, Santa Cruz, Earth and Marine Sciences Building, Santa Cruz, CA 95064, USA.